

C-Band Dual-Polarization Synthetic Aperture Radar Application for Peat Depth Classification: A Case Study in Siak Regency, Riau Province, Indonesia

Dandy A. Novresiandi^{1, *} and Ryota Nagasawa²

Abstract—Knowledge of peat depth distribution is vitally important for accurately estimating carbon stock within tropical peatlands. These estimates aid in understanding the role of tropical peatlands in global environmental change processes. This study evaluates the potential of C-band dual-polarization synthetic aperture radar (SAR) data for peat depth classification on oil palm plantations in Siak Regency, Riau Province, Indonesia. Specifically, features derived after the ground-range radar cross section (sigma-naught or σ^0) and slant-range perpendicular radar cross section (gamma-naught or γ^0) for both polarization channels of C-band Sentinel-1 data were compared and evaluated on monthly basis, during 2015, for discriminating peat depth classes using the decision tree classifier. Overall, γ^0 features yielded a higher value of distance factors (DF) for peat depth classes, for both polarization channels, than those produced by the σ^0 , indicating a better performance in discriminating peat depth classes. Moreover, the seasonal variation of rainfall intensity was discovered to be influencing feature selection for peat depth classification. Thus, the combination of γ^0 features derived in the much rain months was selected for separating the shallow- and medium-peat classes, whereas those derived in the less rain months was selected for discriminating the deep- and very deep-peat classes. In addition, the developed methodology gave the best accuracy for the very deep-peat class, with 76% and 67.86%, producer's accuracy (PA) and user's accuracy (UA), respectively, followed by the shallow-peat class that yielded a PA of 64% and UA of 80%. Subsequently, the deep-peat class produced a PA of 58% and UA of 59.18%, whereas the medium-peat class yielded the lowest PA and UA, of 54% and 49.09%, respectively. This study showed that the C-band dual-polarization SAR data have potential for classifying peat depth classes, particularly on oil palm plantations, and might serve as an efficient tool in peat depth classification used for sustainable management of tropical peatlands.

1. INTRODUCTION

The importance of tropical peatlands as a long-term carbon sinks and stores, as well as their tendency to become a short-term source of carbon emissions, has been receiving tremendous interest during the past two decades [1, 2]. Thus, there is an urgent need to quantify the current carbon status of tropical peatlands to understand their role in relation to the global carbon cycle [3]. It is also important to obtain information about peat depth distribution to be able to accurately estimate carbon stock within tropical peatlands, further aiding in understanding the role of tropical peatlands in global environmental change processes [4]. In general, the distribution of peat depth can be obtained by doing manual sampling using a peat auger, an example of in situ measurements [5]. Nevertheless, this method presents a considerable challenge because conducting extensive in situ measurements at regional, national and global scales is not realistic [6]. Knowledge of peat depth can sometimes be correlated with properties

Received 29 June 2017, Accepted 14 September 2017, Scheduled 9 October 2017

* Corresponding author: Dandy Aditya Novresiandi (dandyaditya@gmail.com).

¹ United Graduate School of Agricultural Sciences, Tottori University, Japan. ² Faculty of Agriculture, Tottori University, Japan.

that are discernible by using a remote sensing (RS) application [7]. However, little is known regarding the performance of RS applications for peat depth distribution classification, especially in the tropics.

RS applications can serve as advantageous tools for tropical peatlands monitoring activities, such as peat depth classification, due to periodic monitoring at various spatial and temporal scales, particularly when combined with field measurement data [4]. Furthermore, the recent development of synthetic aperture radar (SAR)-based RS satellites has introduced a new prospect that allows continuous monitoring and cloud-free observations in humid tropical regions [8]. Recently, the use of SAR-based RS applications for peatlands monitoring activities has been increasing rapidly, along with the growing availability of SAR data sets. A previous study evaluated the potential of X-band dual-polarization SAR data and fusion images with optical data to characterize different peat depths categories in Central Kalimantan, Indonesia [9]. Another report demonstrated the use of L-band Phased Array type L-band SAR (PALSAR) for wide-area mapping of tropical forest and land cover, including several categories for tropical peatlands on Borneo Island [10]. Other reports have evaluated the performance of L-band PALSAR for peatlands detection and delineation in the boreal regions [11, 12]. A previous report also applied the L-band PALSAR to examine a radar scattering mechanism on tropical peatlands in Central Kalimantan, Indonesia [13]. Another study examined the combination of L-band PALSAR data, optical data and digital elevation model (DEM)-derived data for mapping the extent of tropical peatlands in Cuvette Centrale, Congo Basin [14]. Despite all the previous research, detailed information is lacking on the potential C-band dual-polarization SAR data have for classifying peat depth distribution within the tropical peatlands.

The C-band Sentinel-1 data provided by the European Space Agency (ESA) are of interest because they are freely available and have global coverage. The Sentinel-1 mission encompasses a constellation of two polar-orbiting satellites (Sentinel-1A and Sentinel-1B). This data collection method operates at a center frequency of 5.405 GHz and includes two polarization channels — vertical transmit-horizontal receive (VH) and vertical transmit-vertical receive (VV) — with a very short repeat cycle (12 days with one satellite and 6 days with two) and rapid product delivery. These characteristics make C-band Sentinel-1 data particularly promising for use in tropical peatlands monitoring activity, particularly for classifying peat depth distribution. Therefore, in this study, the potential of C-band Sentinel-1 data was evaluated for peat depth classification on oil palm plantations in Siak Regency, Riau Province, Indonesia. Particularly, features derived after the ground-range radar cross section (σ^0) and slant-range perpendicular radar cross section (γ^0) for both polarization channels of C-band Sentinel-1 data were compared and evaluated, monthly during 2015, for discriminating peat depth classes using the decision tree (DT) classifier. In addition, the seasonal variation of peat depth classes, from the viewpoint of C-band dual-polarization SAR data, was analyzed for better understanding of the relationship between peat depth classification and seasonal effects. The results and findings of this study could aid in increasing the foundation of knowledge regarding peat depth classification, involving the use of C-band dual-polarization SAR data, to improve the sustainable management of tropical peatlands.

2. MATERIALS

2.1. Study Area

In Indonesia, there are 14.91 million ha of tropical peatlands that distributed along the low altitudes in the coastal and sub-coastal areas of Sumatra (6.44 million ha, 43%), Kalimantan (4.78 million ha, 32%) and Papua (3.69 million ha, 25%) [15]. Riau Province in Sumatra dominates the provincial level of tropical peatlands distribution, consisting of around 3.86 million ha (26%). This study considers the area of Siak Regency, a rapidly developing region in the central part of Riau Province, where the tropical peatlands have been intensively converted into mostly oil palm and timber plantations over the last two decades [16, 17]. In general, this area has a flat topography and low altitude ranging from 2 to 10 m above sea level. The average temperature of this area is around 26.2°C per year, with an annual rainfall that varies from 2200 to 2600 mm per year. However, in 2015, this area was affected by a very strong El Niño, leading to rainfall anomalies and a more severe dry season [18].

Four study areas, 1×1 km in size, were selected to represent the condition of tropical peatlands in Siak Regency, Riau Province, Indonesia (Fig. 1). These study areas are situated in large-scale oil palm plantations with similar types of growing stages. Furthermore, to represent peat depth categories, each

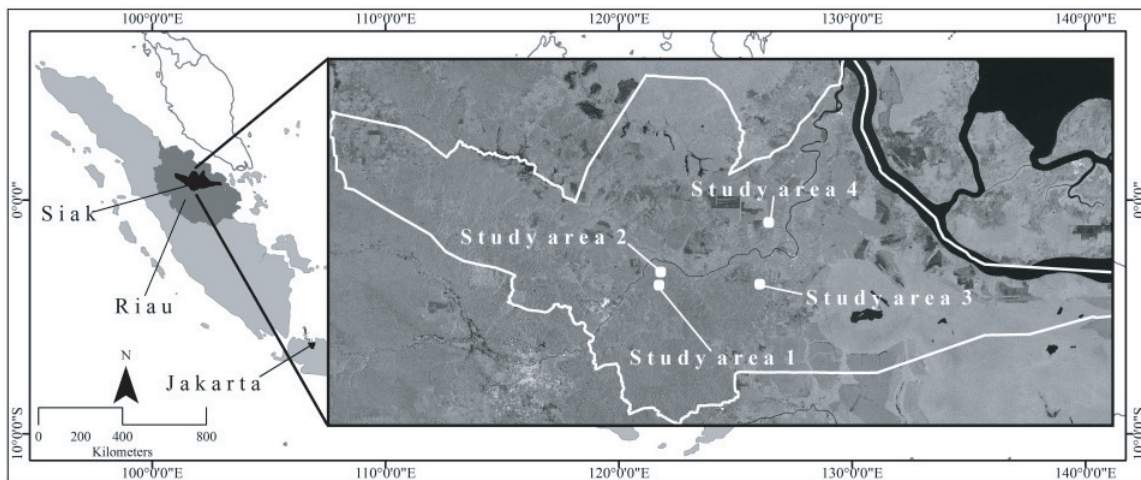


Figure 1. Map of Indonesia showing the location of the study areas in Siak Regency, Riau Province, Indonesia.

study area is located on distinct types of peat depth classes as categorized by the Indonesian Agency for Agricultural Research and Development (IAARD) [15]. Thus, study area 1 is situated in a shallow-peat class (0.5 to 1 m of peat depth), study area 2 is situated in a medium-peat class (1 to 2 m of peat depth), study area 3 is situated in a deep-peat class (2 to 4 m of peat depth), and study area 4 is situated in a very deep-peat class (more than 4 m of peat depth).

2.2. Data

In this study, there were 12 scenes of C-band Sentinel-1 data, acquired between January and December 2015, served as 12-months observations. Thus, each scene, with a specific acquisition date, was used to represent a monthly observation to provide monthly analyses. These scenes were used as the primary data. The C-band Sentinel-1 data were collected using the settings of level-1 Ground Range Detected (GRD) and the acquisition mode of Interferometric Wide (IW) swath [19]. Moreover, Tropical Rainfall Measuring Mission (TRMM) 3B43 version 7 data were used to calculate the amount of monthly rainfall in the study areas [20]. Landsat 8 Operational Land Imager (OLI) data and high-resolution satellite images on Google Earth were used to obtain basic information of the study areas by means of visual interpretation and to select training and testing points for DT classification. A total of 600 points (150 points for each study area) were derived for training the algorithm (400 points) and testing the accuracy of the classification results (200 points). Each point was located within a 100×100 m mesh, with manual adjustments made to avoid points situated on plantation roads. These points represented the detected pixels in the C-band dual-polarization SAR imagery. In addition, an existing peat depth and distribution map, provided by the IAARD, was used as reference map. The list of data used for analyses is shown in Table 1.

3. METHODOLOGY

3.1. Image Processing Steps

The C-band Sentinel-1 data were imported into the ESA Sentinel Application Platform (SNAP) software for image processing [21]. First, the data were radiometrically calibrated and converted from digital pixel values to radiometrically-calibrated backscatter by means of a calibration vector provided in the data product. In this study, the C-band Sentinel-1 data were converted to ground-range radar cross section (sigma-naught or σ^0) and slant-range perpendicular radar cross section (gamma-naught or γ^0) values, in decibel units (dB), for both channels of polarization prior to data analyses. Both σ^0 and γ^0 are measures used to express radar backscatter coefficients. However, σ^0 is defined as the radar cross

Table 1. List of data used for analyses carried out in this study.

| Data usage | Source | Acquisition date |
|----------------|---|---|
| Primary data | C-band Sentinel-1 data (Sentinel-1A satellite, dual-polarization) | Jan. 3, 2015 |
| | | Feb. 19, 2015 |
| | | Mar. 4, 2015 |
| | | Apr. 21, 2015 |
| | | May 15, 2015 |
| | | Jun. 8, 2015 |
| | | Jul. 26, 2015 |
| | | Aug. 18, 2015 |
| | | Sep. 11, 2015 |
| | | Oct. 6, 2015 |
| | | Nov. 11, 2015 |
| | | Dec. 29, 2015 |
| | TRMM 3B43 version 7 (Monthly 0.25×0.25 degree, mm/hour of rainfall rate) | Monthly data between January and December 2015 |
| Secondary data | Landsat 8 OLI | Jul. 10, 2015 |
| | | Jul. 26, 2015 |
| | | Aug. 2, 2015 |
| | | Jul. 25, 2014 |
| | | Jul. 5, 2015 |
| | High-resolution satellite images accessed on Google Earth | Aug. 26, 2016 |

section per unit area in the ground-range, whereas γ^0 is defined as radar cross section per unit area of the incident wavefront (perpendicular to the slant-range), to minimize the incidence angle dependency of the radar backscatter for a distributed target [22, 23].

Furthermore, the data were terrain corrected using SRTM DEM 3 arc-seconds [24] and geocoded to the Universal Transverse Mercator (UTM) zone 48-north map projection with pixel spacing of 10×10 m. Speckle noise was reduced by applying a 7×7 window size Lee filter [25]. In addition, to provide rainfall information for the study areas, the precipitation layers of TRMM 3B43 version 7 data acquired between January and December 2015 were extracted. Rainfall rate conversions from mm/hour to mm/month were calculated. The data were then subset into the boundaries of the study areas so that monthly rainfall information could be generated for the analyses carried out in this study.

3.2. Feature Description

In this study, the σ^0 and γ^0 images, for both polarization channels, derived using the C-band Sentinel-1 data, were considered as features. To allow for monthly analysis, each σ^0 or γ^0 image for a particular polarization channel on a specific acquisition date was considered as one feature (e.g., a σ^0 image for the VH polarization channel acquired on January 3, 2015 was considered as one feature and coded as sVH01; a γ^0 image for the VV polarization channel acquired on November 11, 2015 was considered as one feature and coded as gVV11). Thus, a total of 48 features were derived, using the C-band Sentinel-1 data, for the analyses carried out in this study. The list of features used for analyses is shown in Table 2.

Table 2. List of features used for analyses, derived using sigma naught (σ^0) and gamma naught (γ^0) images, for both polarization channels.

| Polarization channel | Acquisition date | Sigma-naught code name | Gamma-naught code name |
|----------------------|------------------|------------------------|------------------------|
| VH | Jan. 3, 2015 | sVH01 | gVH01 |
| | Feb. 19, 2015 | sVH02 | gVH02 |
| | Mar. 4, 2015 | sVH03 | gVH03 |
| | Apr. 21, 2015 | sVH04 | gVH04 |
| | May 15, 2015 | sVH05 | gVH05 |
| | Jun. 8, 2015 | sVH06 | gVH06 |
| | Jul. 26, 2015 | sVH07 | gVH07 |
| | Aug. 18, 2015 | sVH08 | gVH08 |
| | Sep. 11, 2015 | sVH09 | gVH09 |
| | Oct. 6, 2015 | sVH10 | gVH10 |
| | Nov. 11, 2015 | sVH11 | gVH11 |
| | Dec. 29, 2015 | sVH12 | gVH12 |
| VV | Jan. 3, 2015 | sVV01 | gVV01 |
| | Feb. 19, 2015 | sVV02 | gVV02 |
| | Mar. 4, 2015 | sVV03 | gVV03 |
| | Apr. 21, 2015 | sVV04 | gVV04 |
| | May 15, 2015 | sVV05 | gVV05 |
| | Jun. 8, 2015 | sVV06 | gVV06 |
| | Jul. 26, 2015 | sVV07 | gVV07 |
| | Aug. 18, 2015 | sVV08 | gVV08 |
| | Sep. 11, 2015 | sVV09 | gVV09 |
| | Oct. 6, 2015 | sVV10 | gVV10 |
| | Nov. 11, 2015 | sVV11 | gVV11 |
| | Dec. 29, 2015 | sVV12 | gVV12 |

3.3. Decision Tree (DT) Classification

To classify the peat depth classes using C-band Sentinel-1 data, DT classifier was used due to its ability to handle complex relations among class properties, its computational efficiency and conceptual simplicity [26]. DT is a classification procedure that recursively separates a set of data into smaller subcategories based on a set of rules determined at each branch in the tree. It requires no assumptions regarding the distributions of input data, making it suitable for classifying SAR data [27]. Furthermore, DT algorithm diagrams are explicit and easy to understand, particularly when evaluating feature contributions and relations in a classification procedure [28].

3.4. Distance Factor (DF) Extraction

In this study, the distance factor (DF) was generated to assess the effectiveness of a feature for separating classes, particularly on DT classification. The DF measures the distance between the different class mean values compared to the standard deviations. Thus, if a DF is large, classes are said to be well-separated, according to the concept of feature separation [29]. The DF is defined as:

$$DF_{ij} = \frac{|\bar{x}_i - \bar{x}_j|}{\sigma_i + \sigma_j}, \quad (1)$$

where \bar{x} represents the mean values and σ the standard deviations. The performance of the separation between classes i and j is represented by the value DF_{ij} . A higher DF_{ij} means that a feature has better performance separating the associate class pairs [30]. Thus, in this study, features that yielded the highest DF value on each class pair for each polarization channel were analyzed and applied to the DT algorithm.

In the present study, to apply the concept of feature separation on the DT algorithm, three combinations of class pairs were specified (i.e., (A) “shallow-peat” plus “medium-peat” and “deep-peat” plus “very-deep-peat”, (B) “shallow-peat” and “medium-peat,” and (C) “deep-peat” and “very-deep-peat.” The class pairs were then applied to the DT algorithm to identify each peat depth class. In addition, the selected features for each class pair were analyzed to understand the effect seasonal variation has upon peat depth classifications. Hence, the monthly rainfall information, derived from the TRMM 3B43 version 7 data, was used for seasonal analysis purposes.

3.5. Accuracy Assessment

An accuracy assessment was performed for the classification results using a confusion matrix generated by testing points [31]. Thus, accuracy indicators were derived to evaluate the quality of classification results (i.e., Producer’s Accuracy (PA), User’s Accuracy (UA), Overall Accuracy (OA) and the Kappa coefficient (K)). The PA and UA represent the measures of omission and commission error for each class, respectively. The OA was computed by creating a ratio of the total number of correct pixels to the total number of pixels in the confusion matrix, which correspond to the correctly classified areas of the classified image. Last, the K describes the degree of matching between the reference data set and the classification.

4. RESULTS AND DISCUSSION

4.1. Comparison of σ^0 and γ^0 Features

Table 3 shows the DF values for class pair (A), derived using σ^0 and γ^0 features, for both polarization channels. The values in bold indicate the highest DF values in each category. Generally, the DF values of class pair (A) were varied, depending on the feature used to derive them. The sVH06 (σ_{VH}^0 in June) and sVV06 (σ_{VV}^0 in June) features yielded the highest DF values for those derived using σ_{VH}^0 and σ_{VV}^0 features, respectively. On the other hand, the gVH06 (γ_{VH}^0 in June) and gVV06 (γ_{VV}^0 in June) features produced the highest DF values for those derived using γ_{VH}^0 and γ_{VV}^0 features, respectively.

Thus, by comparing the highest DF values of class pair (A), derived using σ^0 and γ^0 features, for both polarization channels, it was found that γ^0 features yielded much higher DF values for class pair (A), for both polarization channels, than those produced by σ^0 features. By applying γ^0 features, the highest DF values of class pair (A) increased as much as 11.5% and 13.3% for VH and VV polarizations, respectively. Hence, in this study, γ^0 features were used for developing a methodology for classifying peat depth due to the features having better performance in discriminating peat depth classes.

4.2. Selected Features for the Classification

Table 4 shows the DF values for all class pairs, derived by γ^0 features, for both polarization channels. The values in bold indicate the highest DF values in each category. The highest values were selected to be analyzed and applied to the DT algorithm. In general, the DF values for all class pairs varied, depending on the features used to derive them. For class pair (A), as mentioned before, the gVH06 (γ_{VH}^0 in June) and gVV06 (γ_{VV}^0 in June) features yielded the highest DF values for VH and VV polarization, respectively. On the other hand, for class pair (B), the gVH03 (γ_{VH}^0 in March) and gVV04 (γ_{VV}^0 in April) features produced the highest DF values for VH and VV polarization, respectively. Furthermore, for class pair (C), the gVH06 (γ_{VH}^0 in June) and gVV09 (γ_{VV}^0 in September) features generated the highest DF values for VH and VV polarization, respectively. These features were selected and applied to the DT algorithm for classifying peat depth classes.

Table 3. The distance factor (DF) values for class pair (A), derived using sigma naught (σ^0) and gamma naught (γ^0) features, for both polarization channels.

| Feature | | Class pair (A) | |
|----------------------|------------------|----------------|--------------|
| Polarization channel | Acquisition date | Sigma naught | Gamma naught |
| VH | Jan. 3, 2015 | 0.18 | 0.12 |
| | Feb. 19, 2015 | 0.51 | 0.44 |
| | Mar. 4, 2015 | 0.44 | 0.50 |
| | Apr. 21, 2015 | 0.05 | 0.01 |
| | May 15, 2015 | 0.10 | 0.04 |
| | Jun. 8, 2015 | 0.52 | 0.58 |
| | Jul. 26, 2015 | 0.41 | 0.35 |
| | Aug. 18, 2015 | 0.15 | 0.08 |
| | Sep. 11, 2015 | 0.22 | 0.15 |
| | Oct. 6, 2015 | 0.11 | 0.17 |
| | Nov. 11, 2015 | 0.06 | 0.13 |
| | Dec. 29, 2015 | 0.04 | 0.09 |
| VV | Jan. 3, 2015 | 0.06 | 0.12 |
| | Feb. 19, 2015 | 0.40 | 0.33 |
| | Mar. 4, 2015 | 0.41 | 0.46 |
| | Apr. 21, 2015 | 0.19 | 0.25 |
| | May 15, 2015 | 0.03 | 0.02 |
| | Jun. 8, 2015 | 0.45 | 0.51 |
| | Jul. 26, 2015 | 0.04 | 0.11 |
| | Aug. 18, 2015 | 0.31 | 0.24 |
| | Sep. 11, 2015 | 0.32 | 0.25 |
| | Oct. 6, 2015 | 0.32 | 0.37 |
| | Nov. 11, 2015 | 0.09 | 0.15 |
| | Dec. 29, 2015 | 0.00 | 0.07 |

In addition, by examining the highest DF values for all class pairs, derived by γ^0 features, for both polarization channels, it was found that γ_{VH}^0 features produced much higher DF values than those generated by γ_{VV}^0 features, indicating that the γ_{VH}^0 features yielded a better performance in discriminating peat depth classes. However, in this study, all γ^0 features that obtained the highest DF values for both polarization channels were applied to the DT algorithm. Moreover, among all the class pairs, class pair (B) yielded the highest DF values for both polarization channels, indicating that the mean and standard deviation values of the shallow- and medium-peat classes represented in class pair (B) overlapped less, obtaining a higher DF values than those derived in the other class pairs.

4.3. Seasonal Variation of the Selected Features

To understand the effect of seasonal variation on the selected features for peat depth classification, monthly rainfall information derived from the TRMM 3B43 version 7 data was used for seasonal analysis purposes. In 2015, a year with a very strong El Niño, the annual rainfall was as low as 1992 mm, with an average monthly rainfall of 166 mm. For the seasonal analyses carried out in this study, months with below average monthly rainfall were said to be “less rain” months, whereas those

Table 4. The distance factor (DF) values for all class pairs, derived using gamma-naught (γ^0) features, for both polarization channels.

| Feature | | Class pair | | |
|----------------------|-----------|-------------|-------------|-------------|
| Polarization channel | Code name | (A) | (B) | (C) |
| VH | gVH01 | 0.12 | 0.23 | 0.18 |
| | gVH02 | 0.44 | 0.22 | 0.31 |
| | gVH03 | 0.50 | 0.75 | 0.08 |
| | gVH04 | 0.01 | 0.28 | 0.59 |
| | gVH05 | 0.04 | 0.60 | 0.15 |
| | gVH06 | 0.58 | 0.05 | 0.60 |
| | gVH07 | 0.35 | 0.34 | 0.43 |
| | gVH08 | 0.08 | 0.48 | 0.20 |
| | gVH09 | 0.15 | 0.40 | 0.18 |
| | gVH10 | 0.17 | 0.27 | 0.07 |
| | gVH11 | 0.13 | 0.07 | 0.41 |
| | gVH12 | 0.09 | 0.13 | 0.57 |
| VV | gVV01 | 0.12 | 0.34 | 0.28 |
| | gVV02 | 0.33 | 0.48 | 0.44 |
| | gVV03 | 0.46 | 0.62 | 0.55 |
| | gVV04 | 0.25 | 0.71 | 0.04 |
| | gVV05 | 0.02 | 0.65 | 0.42 |
| | gVV06 | 0.51 | 0.38 | 0.05 |
| | gVV07 | 0.11 | 0.38 | 0.29 |
| | gVV08 | 0.24 | 0.50 | 0.51 |
| | gVV09 | 0.25 | 0.48 | 0.56 |
| | gVV10 | 0.37 | 0.30 | 0.48 |
| | gVV11 | 0.15 | 0.36 | 0.12 |
| | gVV12 | 0.07 | 0.28 | 0.07 |

with above average rainfall were said to be “much rain” months. Hence, the less rain months are January (149 mm/month), February (141 mm/month), May (146 mm/month), June (119 mm/month), July (46 mm/month), September (52 mm/month), and October (78 mm/month), whereas the much rain months are March (269 mm/month), August (222 mm/month), November (330 mm/month), and December (254 mm/month).

For class pair (A) (derived by both σ^0 and γ^0), features acquired in June yielded the highest DF value for both polarization channels. Thus, for the initial separation of peat depth classes represented in class pair (A), features derived in the less rain months were prominent. In contrast, for class pair (B), features acquired in March and April produced the highest DF value for VH and VV polarization, respectively. Hence, for more detailed separation of peat depth classes, (i.e., separating the shallow- and medium-peat classes) features derived in the much rain months were suitable. On the other hand, for class pair (C), features acquired in June and September generated the highest DF value for VH and VV polarization, respectively. Therefore, features derived in the less rain months were suitable for separating the deep- and very deep-peat classes. In this study, it was discovered that seasonal variation influenced feature selection for peat depth classification, particularly when analyzing C-band dual-polarization SAR data.

4.4. Results of the Classification

The selected features for peat depth classification were the gVH06 (γ_{VH}^0 in June) and gVV06 (γ_{VV}^0 in June), for separating classes in the class pair (A). Subsequently, the gVH03 (γ_{VH}^0 in March) and gVV04 (γ_{VV}^0 in April) were selected for discriminating peat depth classes in the class pair (B). Afterwards, the gVH06 (γ_{VH}^0 in June) and gVV09 (γ_{VV}^0 in September) were selected for separating peat depth classes in the class pair (C). Thus, a total of three classification rules, separating three class pairs, were generated using training points based on the selected features for peat depth classification. The classification rules were developed using mean and standard deviation values of peat depth classes for each selected feature. These rules are listed as follows:

- (i) Rule 1 for separating classes in the class pair (A).
If gVH06 (γ_{VH}^0 in June) $\geq (-13.20)$ dB and gVV06 (γ_{VV}^0 in June) $\geq (-4.97)$ dB, Then Class pair (B).
- (ii) Rule 2 for separating peat depth classes in the class pair (B).
If gVH03 (γ_{VH}^0 in March) $\geq (-13.55)$ dB and gVV04 (γ_{VV}^0 in April) $\geq (-5.31)$ dB, Then Shallow peat.
- (iii) Rule 3 for separating peat depth classes in the class pair (C).
If gVH06 (γ_{VH}^0 in June) $\geq (-12.71)$ dB and gVV09 (γ_{VV}^0 in September) $\leq (-4.88)$ dB, Then Deep peat.

These classification rules were then applied to the DT algorithm to obtain classification results. The classification rules and DT algorithm diagram developed in this study are shown in Fig. 2. Afterwards, as shown in Fig. 3, results of the peat depth classification of all study areas were successfully generated by means of DT classification. These results presented four peat depth classes (i.e., shallow peat (0.5 to 1 m of peat depth), medium peat (1 to 2 m of peat depth), deep peat (2 to 4 m of peat depth), and very-deep peat (more than 4 m of peat depth)).

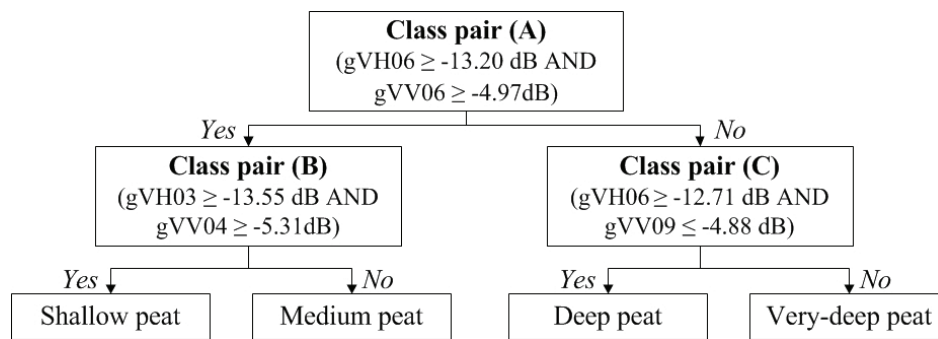


Figure 2. The classification rules and the decision tree (DT) algorithm diagram developed in this study.

Table 5. The pixel percentage of each peat depth class calculated in each study area. The values in bold indicate the highest pixel percentage of peat depth classes produced on each study area.

| Study area | Pixel percentage (%) | | | |
|------------|----------------------|--------------|--------------|----------------|
| | Shallow peat | Medium peat | Deep peat | Very-deep peat |
| 1 | 56.37 | 18.45 | 14.81 | 10.37 |
| 2 | 11.74 | 43.17 | 31.81 | 13.28 |
| 3 | 2.82 | 18.42 | 48.42 | 30.34 |
| 4 | 1.84 | 13.44 | 13.96 | 70.76 |

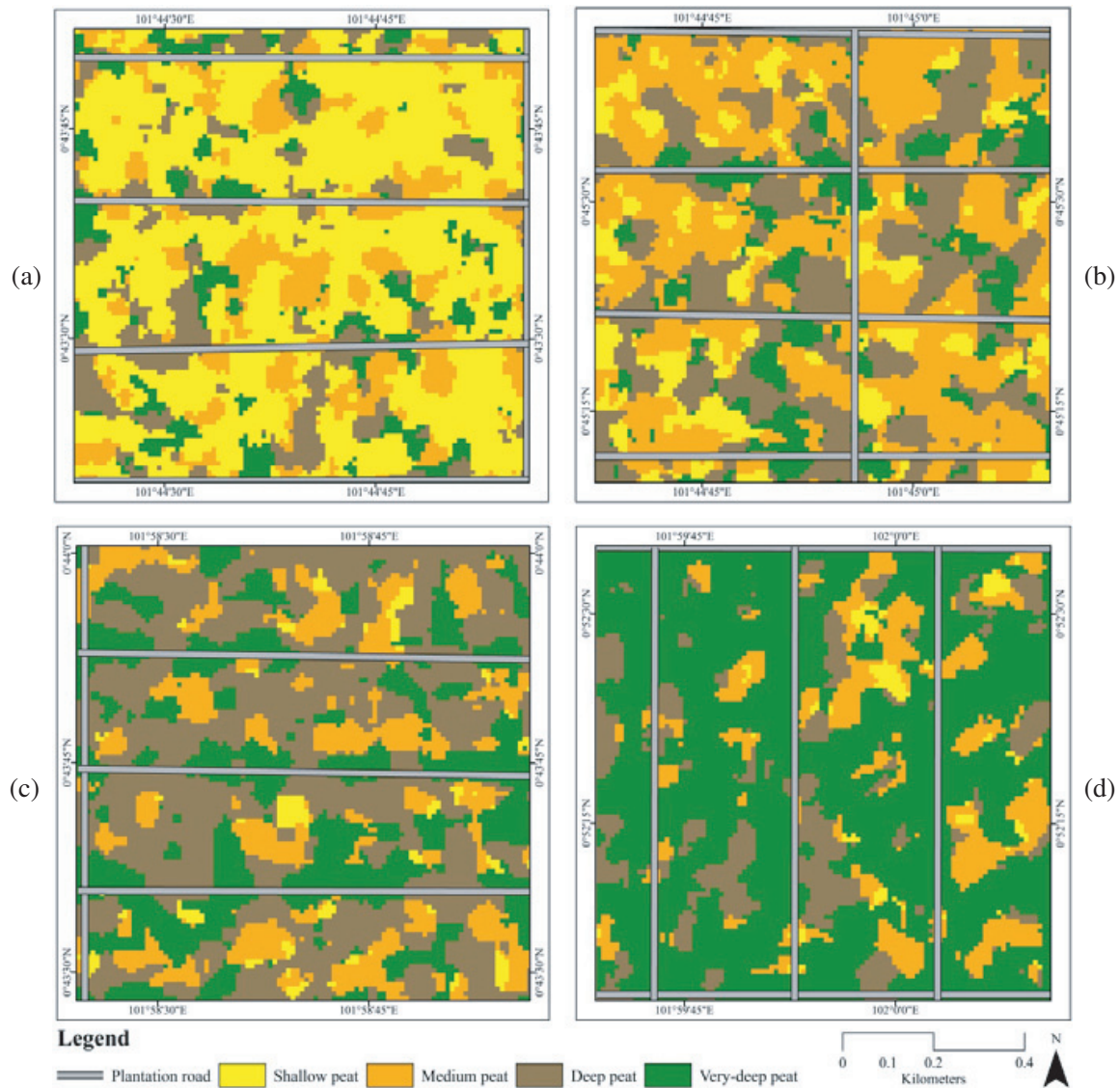


Figure 3. The result of the peat depth classification of (a) study area 1, (b) study area 2, (c) study area 3, and (d) study area 4.

In addition, Table 5 shows the pixel percentage of each peat depth class calculated in each study area. Thus, by comparing the actual peat depth condition of each study area and the pixel percentage of peat depth classes computed on the associated study area, it was found that the developed methodology was always successful in matching the actual peat depth condition with the highest pixel percentage of peat depth classes produced. Hence, in study area 1, an area situated in shallow peat, the highest pixel percentage (56.37%) was yielded for the shallow-peat class. Subsequently, in study area 2, an area situated in medium peat, the highest pixel percentage (43.17%) was produced for the medium-peat class. Next, in study area 3, an area situated in deep peat, the highest pixel percentage (48.42%) was generated for the deep-peat class. Last, in study area 4, an area situated in very deep peat, the highest pixel percentage (70.76%) was yielded for the very deep-peat class. Furthermore, best performance of the developed methodology was found in very deep-peat areas, represented in study area 4, as the methodology generated much higher pixel percentages of peat depth classes that matched with actual peat depth conditions, compared to those derived in other study areas.

4.5. Accuracies of the Classification

Table 6 shows the confusion matrix and accuracy indicators for peat depth classifications by means of DT classification. The accuracy assessment was conducted by using the testing points situated in the study areas, evaluating the performance of the developed peat depth classifications. Thus, the very deep-peat class obtained the best accuracy, with 76% and 67.86%, PA and UA, respectively, followed by the shallow-peat class that yielded a PA of 64% and UA of 80%. Subsequently, the deep-peat class produced a PA of 58% and UA of 59.18%, whereas the medium-peat class yielded the lowest PA and UA, of 54% and 49.09%, respectively. This result showed that the C-band dual-polarization SAR data have potential for classifying peat depth classes, particularly on oil palm plantations, due to its ability to produce the best accuracy for the very deep-peat class that is difficult to be distinguished among peat depth classes [4]. In addition, the developed methodology gave accuracies of 63% and 0.51, for OA and K, respectively. This value of K was considered as a moderate agreement of a classification result [32]. Furthermore, the accuracy assessment result agreed with the analysis result for the pixel percentage of peat depth classes generated on each study area as presented in Section 4.4, whereby the developed methodology consistently gave the best performance for the very deep-peat areas.

Table 6. The confusion matrix and accuracy indicators for peat depth classifications using the decision tree (DT) classification.

| Class | Reference | | | | Total | Producer's Accuracy (%) | User's Accuracy (%) |
|----------------------|--------------|-------------|-----------|----------------|-------|-------------------------|---------------------|
| | Shallow peat | Medium peat | Deep peat | Very-deep peat | | | |
| Shallow peat | 32 | 7 | 1 | 0 | 40 | 64.00 | 80.00 |
| Medium peat | 11 | 27 | 11 | 6 | 55 | 54.00 | 49.09 |
| Deep peat | 3 | 11 | 29 | 6 | 49 | 58.00 | 59.18 |
| Very-deep peat | 4 | 5 | 9 | 38 | 56 | 76.00 | 67.86 |
| Total | 50 | 50 | 50 | 50 | 200 | | |
| Overall Accuracy (%) | 63.00 | | | | | | |
| Kappa coefficient | 0.51 | | | | | | |

5. CONCLUSION

This study evaluated the potential of C-band Sentinel-1 data for peat depth classification on oil palm plantations, by using a SAR-based RS application, in response to the emerging tropical peatlands monitoring activities. Several findings were obtained relating to the development of peat depth classification using C-band dual-polarization SAR data. First, the present study showed that the γ^0 features yielded better performance in discriminating peat depth classes. By comparing the highest DF values of class pair (A), derived using σ^0 and γ^0 features, for both polarization channels, it was found that γ^0 features yielded much higher DF values for class pair (A), for both polarization channels, than those produced by σ^0 features. Thus, by applying γ^0 features, the DF values of class pair (A) increased as much as 11.5% and 13.3% for VH and VV polarizations, respectively. Second, it was discovered that seasonal variation was influencing feature selection for peat depth classification. Both γ_{VH}^0 and γ_{VV}^0 , in the much rain months, were selected for separating the shallow- and medium-peat classes in class pair (B), whereas both γ_{VH}^0 and γ_{VV}^0 , in the less rain months, were selected for discriminating the deep- and

very deep-peat classes in class pair (C). Third, the developed methodology gave the best accuracy for the very deep-peat class, with 76% and 67.86%, producer's accuracy (PA) and user's accuracy (UA), respectively, followed by the shallow-peat class that yielded a PA of 64% and UA of 80%. Subsequently, the deep-peat class produced a PA of 58% and UA of 59.18%, whereas the medium-peat class yielded the lowest PA and UA, of 54% and 49.09%, respectively. Moreover, it was discovered that the developed methodology was always successful in matching the actual peat depth condition with the highest pixel percentage of peat depth classes generated. Furthermore, accuracy assessment results agreed with the analysis results for the pixel percentage of peat depth classes produced in each study area, whereby the developed methodology was consistent in providing the best performance for very deep-peat areas. The results and findings in this study show that the C-band Sentinel-1 data are suitable for classifying peat depth classes, particularly on oil palm plantations, and might serve as an efficient tool in peat depth classification used for sustainable management of tropical peatlands.

REFERENCES

1. Osaki, M., D. Nursyamsi, M. Noor, Wahyunto, and H. Segah, "Peatland in Indonesia," *Tropical Peatland Ecosystems*, M. Osaki and N. Tsuji (eds.), 49–58, Springer, Tokyo, Japan, 2016.
2. Miettinen, J., A. Hooijer, R. Vernimmen, S. C. Liew, and S. E. Page, "From carbon sink to carbon source: extensive peat oxidation in insular Southeast Asia since 1990," *Environmental Research Letters*, Vol. 12, No. 024014, 1–10, 2017.
3. Hirano, T., S. Sundari, and H. Yamada, "CO₂ balance of tropical peat ecosystems," *Tropical Peatland Ecosystems*, M. Osaki and N. Tsuji (eds.), 329–338, Springer, Tokyo, Japan, 2016.
4. Shimada, S., H. Takahashi, and M. Osaki, "Carbon stock estimate," *Tropical Peatland Ecosystems*, M. Osaki and N. Tsuji (eds.), 455–467, Springer, Tokyo, Japan, 2016.
5. Agus, F., K. Hairiah, and A. Mulyani, *Measuring Carbon Stock in Peat Soils: Practical Guidelines*, World Agroforestry Centre (ICRAF) Southeast Asia Regional Program and Indonesian Centre for Agricultural Land Resources Research and Development, Bogor, Indonesia, 2011.
6. Jaenicke, J., J. O. Rieley, C. Mott, P. Kimman, and F. Siegert, "Determination of the amount of carbon stored in Indonesian peatlands," *Geoderma*, Vol. 147, 151–158, 2008.
7. Lawson, I. T., T. J. Kelly, P. Aplin, A. Boom, G. Dargie, F. C. H. Draper, P. N. Z. B. P. Hassan, J. Hoyos-Santillan, J. Kaduk, D. Large, W. Murphy, S. E. Page, K. H. Roucoux, S. Sjögersten, K. Tansey, M. Waldram, B. M. M. Wedeux, and J. Wheeler, "Improving estimates of tropical peatland area, carbon storage, and greenhouse gas fluxes," *Wetlands Ecology Management*, Vol. 23, 327–346, 2015.
8. Kuntz, S., "Potential of spaceborne SAR for monitoring the tropical environments," *Tropical Ecology*, Vol. 51, No. 1, 3–10, 2010.
9. Wijaya, A., P. R. Marpu, and R. Gloaguen, "Discrimination of peatlands in tropical swamp forests using dual-polarimetric SAR and Landsat ETM data," *International Journal of Image Data Fusion*, Vol. 1, No. 3, 257–270, 2010.
10. Hoekman, D. H., M. A. M. Vissers, and N. Wielaard, "PALSAR wide-area mapping of borneo: methodology and map validation," *IEEE Journal of Selected Topics in Applied Earth Observations and Remote Sensing*, Vol. 3, No. 4, 605–617, 2010.
11. Antropov, O., Y. Rauste, J. Praks, M. Hallikainen, and T. Häme, "Peatland delineation under forest canopy with polsar data using model based decomposition technique," *Proceeding IEEE International Geoscience and Remote Sensing Symposium*, 4918–4921, 2012.
12. Antropov, O., Y. Rauste, H. Astola, J. Praks, T. Häme, and M. T. Hallikainen, "Land cover and soil type mapping from spaceborne PolSAR data at L-band with probabilistic neural network," *IEEE Transactions on Geoscience and Remote Sensing*, Vol. 52, No. 9, 5256–5270, 2014.
13. Watanabe, M., K. Kushida, and C. Yonezawa, "PALSAR full-polarimetric observation for peatland," *Asian Journal of Geoinformatics*, Vol. 11, No. 3, 2011.

14. Dargie, G. C, S. L. Lewis, I. T. Lawson, E. T. A. Mitchard, S. E. Page, Y. E. Bocko, and S. A. Ifo, "Age, extent and carbon storage of the central Congo Basin peatland complex," *Nature*, Vol. 542, No. 2, 86–90, 2017.
15. Ritung, S., Wahyunto, and K. Nugroho, "Karakteristik dan sebaran lahan gambut di Sumatera, Kalimantan dan Papua," *Pengelolaan Lahan Gambut Berkelanjutan*, E. Husen, M. Anda, M. Noor, H. S. Mamat, Maswar, A. Fahmi, and Y. Sulaiman (eds.), BBSDLP, Bogor, Indonesia, 2012.
16. Sabiham, S. and S. Kartawisastra, "Peatland management for oil palm development in indonesia," *Indonesian Journal of Land Resources*, Vol. 6, No. 2, 55–66, 2012.
17. Irawan, S. and L. Tacconi, *Intergovernmental Fiscal Transfer, Forest Conservation and Climate Change*, Edward Elgar, Cheltenham, UK, 2016.
18. Enghart, S., M. Staengel, and F. Siegert, "Estimation of fire affected areas and carbon emissions on the basis of Sentinel-1," *Proceedings of the 15th International Peat Congress 2016: Poster Presentations*, 370–374, Kuching, Sarawak, Malaysia, 2016.
19. Dimov, D., J. Kuhn, and C. Conrad, "Assessment of cropping system diversity in the Fergana Valley through image fusion of Landsat 8 and Sentinel-1," *ISPRS Annals of the Photogrammetry, Remote Sensing and Spatial Information Sciences*, Vol. III-7, 173–180, 2016.
20. Huffman, G. J., R. F. Adler, D. T. Bolvin, and E. J. Nelkin, "The TRMM Multi-satellite Precipitation Analysis (TMPA)," *Satellite Rainfall Applications for Surface Hydrology*, F. Hossain and M. Gebremichael (eds.), 3–22, Springer Verlag, 2010.
21. Luis, V., J. Lu, M. Fomelis, and M. Engdahl, "ESA's multi-mission Sentinel-1 Toolbox," *Proceedings of the 19th EGU General Assembly*, 19398, Vienna, Austria, 2017.
22. Shimada, M., "Ortho-rectification and slope correction of SAR data using DEM and its accuracy evaluation," *IEEE Journal of Selected Topics in Applied Earth Observations and Remote Sensing*, Vol. 3, No. 3, 657–671, 2010.
23. El-Darymli, K., P. McGuire, E. Gill, D. Power, and C. Moloney, "Understanding the significance of radiometric calibration for synthetic aperture radar imagery," *Canadian Conference on Electrical and Computer Engineering*, Toronto, Canada, 2014.
24. Farr, T. G., et al., "The shuttle radar topography mission," *Reviews of Geophysics*, Vol. 45, No. 2, RG2004, 2007.
25. Lee, J. and E. Pottier, *Polarimetric SAR Radar Imaging: From Basic to Applications*, CRC Press, Taylor & Francis Group, 2009.
26. Friedl, M. A. and C. E. Brodley, "Decision tree classification of land cover from remotely sensed data," *Remote Sensing of Environment*, Vol. 61, 399–409, 1997.
27. Simard, M., S. S. Saatchi, and G. D. Grandi, "The use of decision tree and multiscale texture for classification of JERS-1 SAR data over tropical forest," *IEEE Transactions on Geoscience and Remote Sensing*, Vol. 38, No. 5, 2310–2321, 2000.
28. Simard, M., G. D. Grandi, S. Saatchi, and P. Mayaux, "Mapping tropical coastal vegetation using JERS-1 and ERS-1 radar data with a decision tree classifier," *International Journal of Remote Sensing*, Vol. 23, No. 7, 1461–1474, 2002.
29. Cumming, I. G. and J. J. Van Zyl, "Feature utility in polarimetric radar image classification," *Proceeding IEEE International Geoscience and Remote Sensing Symposium*, 1841–1846, 1989.
30. Chen, J., H. Lin, and Z. Pei, "Application of ENVISAT ASAR data in mapping rice crop growth in southern China," *IEEE Geoscience and Remote Sensing Letters*, Vol. 4, No. 3, 431–435, 2007.
31. Congalton, R. G., "A review of accessing the accuracy of classifications of remotely sensed data," *Remote Sensing Environment*, Vol. 37, 35–46, 1991.
32. Viera, J. A. and J. M. Garrett, "Understanding interobserver agreement: The kappa statistic," *Family Medicine*, Vol. 37, No. 5, 360–363, 2005.